



## Adsorption of cationic methylene blue dye on polystyrene sulfonic acid composites from waste: Kinetics and equilibrium

Hemat M. Dardeer<sup>a</sup>, Ragab E. Abouzeid<sup>b,\*</sup>, Mohamed Y. Mahgoub<sup>a</sup>, Adel Abdelkader<sup>a</sup>

<sup>a</sup>Chemistry Department, Faculty of Science, South Valley University, Qena 83523, Egypt

<sup>b</sup>Cellulose and Paper Department, National Research Centre, 33 El-Bohouth st., Dokki, P.O. 12622, Giza, Egypt



CrossMark

### Abstract

In this study a unique polystyrene sulfonic acid (PSSA) has been synthesized by chemical recycling of waste expanded polystyrene used for fridge packing. Polystyrene sulfonic acid has been used for the preparation of polystyrene composites with silicon dioxide in three percentages 5%, 10%, and 20%. FT-IR, <sup>1</sup>H-NMR, and <sup>13</sup>C-NMR spectroscopic analysis of the obtained materials confirmed their structure. Scanning electron microscopy (SEM) was used to examine the surface morphology of the prepared materials. The crystallinity of the polymer composite was observed through XRD (X-ray diffraction) techniques, and its thermal stability with thermogravimetry (TG) processes was studied. Furthermore, polystyrene sulfonic acid and its composites with silicon dioxide were used as solid adsorbents for decontaminating organic dye-contaminated water. PSSA/Silicon dioxide composites could regenerate the methylene blue MB for a maximum of four cycles without losing their adsorption efficiency.

Keywords: Polystyrene sulfonic acid; Silicon dioxide; Adsorption; Dyes

### 1. Introduction

Water pollution from dye wastewater generated by the textile industry is a major threat to human health. Dyeing with organic substances reduces light diffusion into aquatic environments, altering photosynthesis and disrupting ecological balance [1,2]. All forms of life are at risk when organic pollutants are discharged directly into ground water systems [3,4]. Adsorption is one of the recent technologies and most effective methods at low concentrations for removing organic contaminants from wastewater. In addition to their beneficial properties, such as high uptake capacity and fast kinetics, adsorption has proven to be a promising technology [5–8]. At low concentrations, adsorption is one of the most effective methods for removing contaminants from wastewater. There are some challenges when it comes to traditional adsorption technologies used in water purification, including high energy costs, low selectivity, and the production of secondary contaminants [9,10]. Nevertheless, it is a reasonable method with low probability of secondary pollutants release when used for organic pollutant elimination. At present time polymers have become the most essentially materials for science and industrial development. The modern society cannot

live or progress without polymers. Because polymers have many applications in different daily fields in addition to polymers are low cost and can be easily fabricated to consumer products. They have been commonly used in the form of packaging materials for farm, forest, dairy products, and other consumer items. Nevertheless, when discarded after use, they pose a threat to environmental pollution [11,12]. Recent advances in adsorption technology addressing using biodegradable and sustainable natural polymers such as cellulose [13–18] chitosan [19–22], ionic chitosan/silica [23], alginate [24–26] and starch [27], oxidized alginate/gelatin decorated silver nanoparticles [25]. For oil water separation, cellulose nanocrystals and polyvinylidene fluoride (PVDF) nanofibers [28,29] and bacterial cellulose and crosslinked cellulose nanofibers membranes were used [30]. The wide use of polymeric materials leads to the waste removal management difficulties. Land filling of plastics is not favored due to space constraints and land pollution. Furthermore, the decomposition of polymer chain leads to increase of emission of toxic gases. Polymer industry both manufacturing and processing have a positive threat to the environment when these industrial operations proceed without controlling. The worldwide

\*Corresponding author e-mail: [r\\_abouzeid2002@yahoo.com](mailto:r_abouzeid2002@yahoo.com); (Ragab Abouzeid).

Receive Date: 04 November 2021, Revise Date: 21 December 2021, Accept Date: 27 December 2021

DOI: 10.21608/EJCHEM.2021.104402.4822

©2022 National Information and Documentation Center (NIDOC)

production of plastics is 150 million tons per year, and polystyrene (PS) constitutes around 10 % of it [31,32]. The problem of disposal of waste plastics is complex, and requires active participation of industry, government and the public. Among the plastics pollutants, polystyrene is used extensively with several applications. The demands and tremendous growth of PS will continue in the future and it is expected that PS will grow by 5 % each year till 2025 [33,34]. Polystyrene is widely used in numerous areas, including packaging, food containers, electronics, and building materials [35]. The huge production leads to enormous polystyrene waste formation. Currently, the main methods applied in plastic waste treatment are landfill, incineration, mechanical recycling, and chemical recycling. Chemical recycling might be the best treatment for polystyrene waste since it has less environmental impact, and is able to recover the useful materials that polystyrene waste contained [8,22]. In this study, we try to combine two important goals. The first one, is to convert the waste expanded polystyrene to a more valuable functional polymer, i.e., polystyrene sulfate and composite. As a second goal, these materials will be used to remove methylene blue dye from aqueous solutions based on the initial concentration and pH. To confirm their efficiency as sustainable adsorbents, the equilibrium and kinetic models were applied to investigate their adsorption properties towards MB.

## 2. Experimental section

### 2.1. Materials

The waste expanded polystyrene (EPS) obtained from cushioning packages used to protect equipment's during shipment, e.g. refrigerators) was used without any further purification. An acidic solution (95%) of sulfuric acid was used as a sulfonating agent (purchased from PROLABO) and quartz from South Valley University's geology department was used. The raw EPS were first washed by water and dried at 50°C overnight in the oven.

### 2.2. Procedure

#### 2.2.1. Synthesis of polystyrene sulfonic acid from waste expanded polystyrene (1)

Waste expanded polystyrene used for the preparation of PSSA was obtained from polystyrene foam used as cushioning for packing fridges. 50 g of polystyrene waste was dissolved in 100 ml of chloroform until complete solubility, 12 ml of concentrate sulfuric acid was added to polystyrene solution drop by drop with continuous stirring at 50°C for 4 hours. The colour of the reaction mixture was converted to grey with increasing the viscosity of the mixture. The formed polymer was dried in petri dish for two days at room temperature. The precipitate formed was washed many times with distilled water until a neutral filtrate was obtained, then recrystallized from commercial ethanol.

The polymer formed was then dried and its acidity was determined by titration with 1M aqueous NaOH and followed by back titrated with 1M HCl using phenolphthalein as an indicator.

#### 2.2.2 General procedure for the Synthesis of polystyrene sulfonic acid/ composites (2-4)

Quartz is grinded with an electric grinder into a fine powder. PSSA-loaded quartz (or silica) adsorbents were prepared by sequential incipient wetness impregnation method. Pure quartz powder samples were loaded with x% (w/w) of PSSA (where x = 5%, 10%, or 20%) using known volumes of x% (w/v) solution of PSSA in chloroform. The resulted final pastes were dried at 100°C for 12 hours, and then it was stored in glass containers.

### 2.3. Characterizations

#### 2.3.1. Characterization techniques

X-ray powder diffraction analysis (XRD) of the samples was carried out using an X-ray diffractometer (Rigaku RU-200A) operated at 40 kV and 30 mA with CuK $\alpha$  radiation using monochromator. The FT-IR spectra (KBr) were recorded on a Shimadzu 408 spectrometer and carried out at the Central laboratory of South Valley University. <sup>1</sup>H-NMR spectra were recorded using 400 MHz Varian EM 390 spectrometer; chemical shifts are reported in ppm with TMS as an internal standard and are given in  $\delta$  units. The surface morphology of the prepared polystyrene sulfonic acid and their composites was evaluated using a scanning electron microscope, (JSM-5500 LV, SEM, JEOL, Japan). TG analysis was performed at a heating rate of 15°C/min in a flow of 40 cm<sup>3</sup>/min dry nitrogen, using automatically recording model 50H Shimadzu thermal analyzer, Japan. The thermal analyzer is equipped with a data acquisition and handling system (TA-50WSI).

#### 2.4. Adsorption studies

Stocks (2000 ppm) of MB were diluted with water to prepare aqueous solutions of MB at various initial concentrations. The general experimental procedure was as follows: PSSA and PSSA/SiO<sub>2</sub> composite was adjusted to a concentration and time interval appropriate to 50 mL MB solution. Using a spectrophotometer (UNICO UV-2000), aliquots of the suspension were measured at maximum absorbance (670 nm). Batch adsorption techniques consisted of the application of known amounts of PSSA and PSSA/SiO<sub>2</sub> composite at definite times and pH levels. Using the equation below, we calculated the amount of adsorbed MB dye on PSSA and PSSA/SiO<sub>2</sub> composites at equilibrium,  $q_e$  (mg/g):

$$q_e = ((C_0 - C_e)V)/W \quad (1)$$

$C_0$  and  $C_e$  represent the initial and equilibrium dye concentrations on PSSA (mg/L),  $V$  is the volume (L) of dye solution used in the adsorption experiment, and  $W$  represents the weight of PSSA and PSSA/SiO<sub>2</sub> (g).

### 3. Results and discussion

#### 3.1. Synthesis and spectral analysis of the prepared PSSA composites

Scheme 1 presents the procedure employed for the synthesis of the PSSA (1) and PSSA/SiO<sub>2</sub> (2-4). Polystyrene sulphonic acid was prepared by chemical recycling of waste expanded polystyrene by sulphonating using concentrated sulphuric acid in chloroform. Polystyrene composites PSSA/SiO<sub>2</sub> quartz were prepared by impregnation method in three percentage 5, 10 and 20 %. The chemical structure of PSSA confirmed by <sup>1</sup>H-NMR and <sup>13</sup>C-NMR figure 1 A, B. <sup>1</sup>H-NMR spectra in CDCl<sub>3</sub> indicated that presence of two peaks at 1.48 ppm and 1.88 ppm for polystyrene chain. Also showed that appearance a single peak at  $\delta$  2.09 ppm for (SO<sub>3</sub>H) group and aromatic protons at 6.41-7.28 ppm. <sup>13</sup>C-NMR spectrum of PSSA in CDCl<sub>3</sub> established the chemical structure of the polymer, thus, there are different peaks due to the aliphatic carbon chain at 40.39, 42.53, 43.88, 44.23, and 45.90 ppm. Also, the aromatic carbons appear at chemical shift 125.66, 127.68, 127.98, and 145.31 ppm respectively.

#### 3.2. FTIR analysis

The FTIR spectra give good indication for the preparation of PSSA and their composites with quartz. The resulting polymers were characterized by FTIR spectra, Table 1 summarizes the frequencies of PSSA (1) and PSSA/ quartz (2). FTIR spectrum of PSSA shows that aliphatic protons at 2932 cm<sup>-1</sup>, CH aromatic protons at 3035 cm<sup>-1</sup>. Also, indicates presence of (S=O) group at 1359 cm<sup>-1</sup> and (C=C) aromatic' absorption band at about 1558 cm<sup>-1</sup>. The FTIR spectrum of quartz indicates of peak due to Si-O bending at 802.55 cm<sup>-1</sup>, peak due to Si-OH stretching at 938.34 cm<sup>-1</sup> and peak due to Si-O-Si stretching at 1083.25 cm<sup>-1</sup> [36] (Figure 2). Table 1 shows the difference in the intensity of PSSA before and after loaded onto quartz. The shift is due to the formation of polymer composites (2-4). The decreasing in frequencies are due to the formation of Vander Waals forces and hydrogen bonds between the hydroxyl groups of PSSA and quartz. Table 1 display the change in the absorption bands of PSSA (1) after formation of the polymer composites (3, 4). Accordingly, FTIR spectra of PSSA/SiO<sub>2</sub> (3) reveals band at 3423 cm<sup>-1</sup> for hydroxyl groups, characteristic band due to CH aliphatic at 2926 cm<sup>-1</sup>, appearance of characteristic stretching band for SiO<sub>2</sub> at 1037. Both of  $\nu$ [OH] symmetric stretching and  $\nu$ [SO<sub>2</sub>] were shifted to higher frequency. On the other hand,  $\nu$ [CH-aliphatic] and  $\nu$ [CH-aromatic] were shifted to lower frequency due to the introducing of SiO<sub>2</sub> the on the PSSA (1). FTIR spectra of PSSA/SiO<sub>2</sub> (4) shows band at 3431 cm<sup>-1</sup> for hydroxyl groups, CH aliphatic at 2926 cm<sup>-1</sup>, appearance of band for SiO<sub>2</sub> at 1074. The frequencies of  $\nu$ [OH] symmetric stretching,  $\nu$ [SO<sub>2</sub>],  $\nu$ [CH-

aromatic] and  $\nu$ [C=C] were shifted to higher frequency. On the other hand,  $\nu$ [CH-aliphatic] was shifted to lower frequency due to insertion of SiO<sub>2</sub> the on the PSSA (1).

#### 3.3. SEM morphology

In Figure 3, we illustrate the morphology and elemental distribution of PS, PSSA, and PSSA/5%SiO<sub>2</sub>, PSSA/10%SiO<sub>2</sub> and PSSA/20%SiO<sub>2</sub> nanocomposite. Using scanning electron microscopy, a smooth and homogenous surface was observed, indicating that PSSA/SiO<sub>2</sub> particles are homogeneously dispersed in the matrix. PSSA/SiO<sub>2</sub> containing sulphonic acid group nanocomposite was further confirmed by EDX analysis. Besides the signals derived from carbon and oxygen, the formed nanocomposite also has signals derived from silicon and sulfur. Nanocomposite formed using silicon shows high silicon content in the EDX spectrum. As a result of their elemental distribution, the prepared hybrid materials confirm that their homogeneity and stability are not affected by temperature changes. A major contribution towards understanding the degree of structural homogeneity of hybrid systems is the analysis of elemental distributions and concentrations of silicon (inorganic network former).

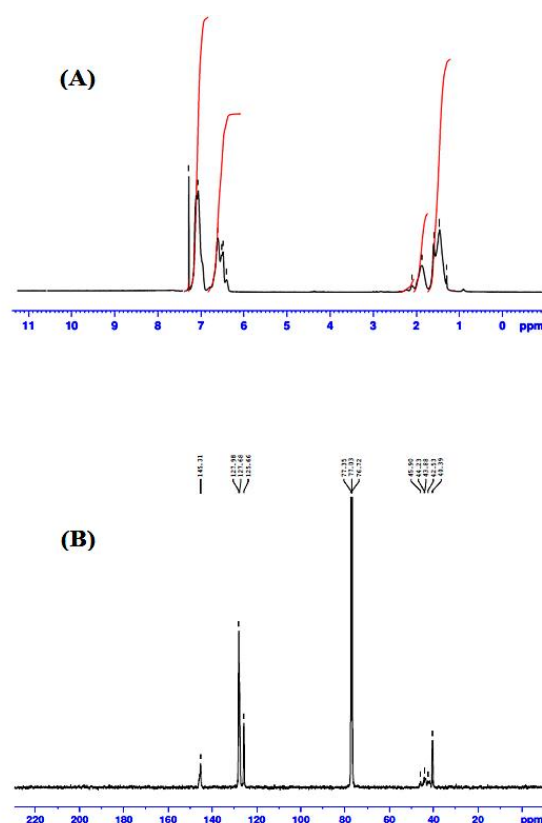


Fig. 1. (A) <sup>1</sup>H-NMR spectra and (B) <sup>13</sup>C-NMR spectra of polystyrene sulphononic acid from waste in CDCl<sub>3</sub>

**Table 1:** Kinetic parameters for MB adsorption by PSSA and PSSA/SiO<sub>2</sub> composites.

	Pseudo first order parameters				Pseudo second order parameters		
	qe.exp (mg/g)	qe.cal (mg/g)	K1(min <sup>-1</sup> )	R2	qe.cal(mg/g)	K2 (g(mg min) <sup>-1</sup> )	R2
PSSA	78	48	0.039	0.90	87	7.5x 10 <sup>-4</sup>	0.991
PSSA/SiO <sub>2</sub>	84	67	0.044	0.97	94	7.4 x 10 <sup>-4</sup>	0.996

**Table 2** Parameters for MB adsorption by PSSA and PSSA/SiO<sub>2</sub> according to different equilibrium models.

	Langmuir isotherm parameters			Freundlich isotherm parameters		
	Ks (mg/L)	qm(mg/g)	R2	P (mg/g)	n	R2
PSSA	140	400	0.982	10.7	1.74	0.725
PSSA/SiO <sub>2</sub>	84	434	0.916	18.7	1.97	0.718

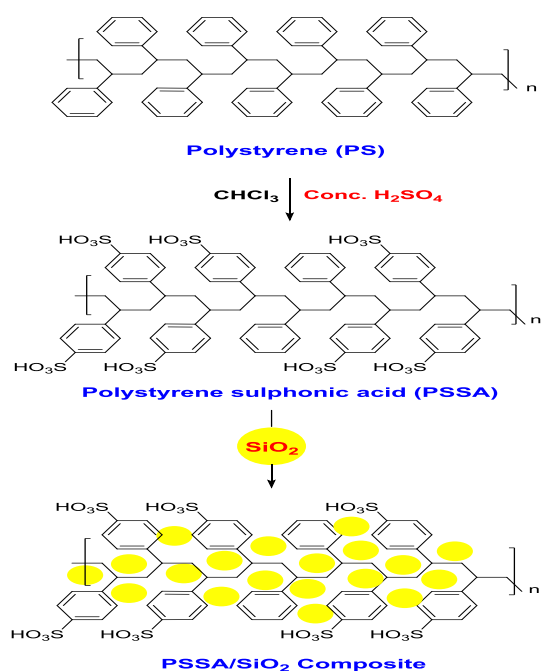
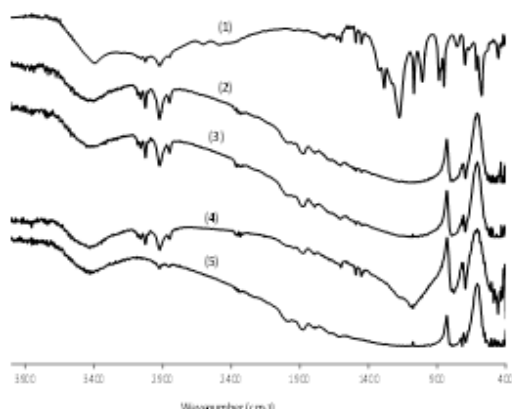
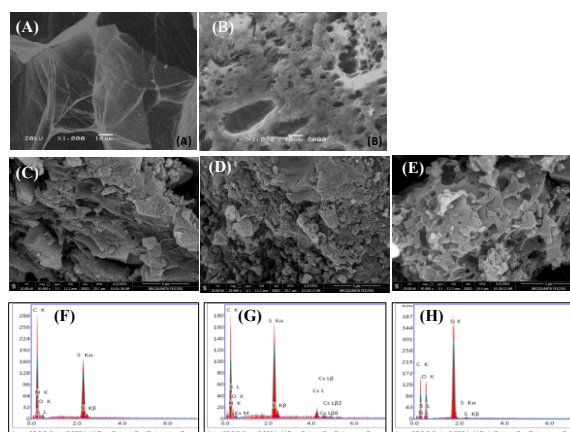
Scheme 1. Synthetic method for the preparation of PSSA and PSSA/SiO<sub>2</sub> composites

Fig. 2: FTIR- spectra for PSSA (1), PSSA/quartz 5% (2), PSSA/quartz 5% (3), PSSA/quartz 5% (4) and quartz (5)

### 3.4. X-ray diffraction

Figure 4 shows the X-ray diffraction pattern for PSSA and PSSA with different SiO<sub>2</sub> concentrations. There is a broad noncrystalline diffraction peak at 2θ of about 10° and 19° consistent with amorphous polymer PSSA. PSSA/5% SiO<sub>2</sub>, PSSA/10% SiO<sub>2</sub>, and PSSA/20% SiO<sub>2</sub> exhibited characteristic peaks at 2θ values of 20°, 26°, 36°, 39°, 50°, 55°, 59° and 68° (figure 4). The peaks correspond to the quartz crystal form of SiO<sub>2</sub>.

Fig. 3: SEM images (A) PS, (B) PSSA, (C) PSSA/5%SiO<sub>2</sub> (D) PSSA/10%SiO<sub>2</sub> and (E) PSSA/20%SiO<sub>2</sub>. EDX spectra (F) PSSA/5%SiO<sub>2</sub> (G) PSSA/10%SiO<sub>2</sub> (H) PSSA/20%SiO<sub>2</sub> nanocomposite.

### 3.5. Adsorption studies

#### 3.5.1. Effect of pH on the adsorption capacity

As shown in Figure 5, pH has an effect on the adsorption of methylene blue dye by PSSA and PSSA/SiO<sub>2</sub> (10%). In the case of PSSA and PSSA/SiO<sub>2</sub> (10%), it was shown that pH significantly increased adsorption capacities, which were 78 and 84 mg/g, respectively, when pH was increased to neutral pH (pH 7.0). As the surface property of the sponge and the dye's ionization level are influenced by pH, the pH

controls the retention of dye. Upon increased pH, PSSA and PSSA/Silica (10%) are deprotonated and contrarious charged. This may result in higher absorption of the dye due to the attraction of emphatically charged MB particles.

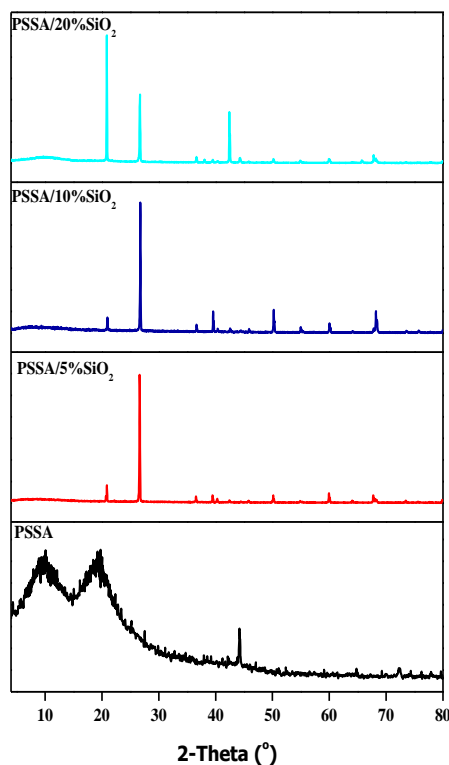


Fig. 4 XRD of PSSA, and PSSA with different percent of SiO<sub>2</sub>.

### 3.5.2. Adsorption kinetics and the effect of contact time

$$\log(q_e - q_t) = \log(q_e) - \frac{K_1}{2.303} t \quad \text{Eq. (2)}$$

$$\frac{t}{q_t} = \frac{t}{q_e} + \frac{1}{K_2 q_e^2} \quad \text{Eq. (3)}$$

A time of adsorption is represented by  $q_t$  (mg/g), while an equilibrium adsorption is represented by  $q_e$  (mg/g).  $k_1$  (min<sup>-1</sup>) and  $k_2$  (g mg<sup>-1</sup>min<sup>-1</sup>) are the rate constants for the pseudo-first and pseudo-second models, respectively.

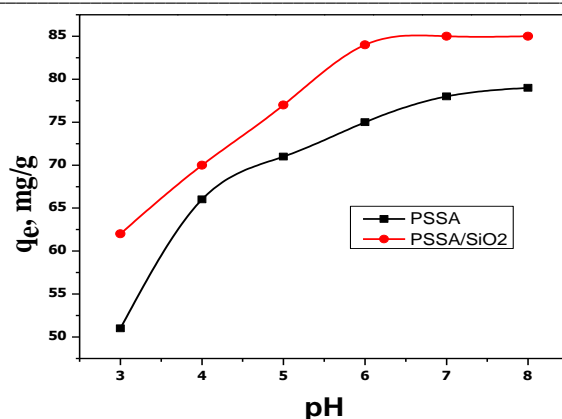


Fig. 5. Effect of pH on the adsorption capacities of PSSA and PSSA/10 % SiO<sub>2</sub> / for MB dye.

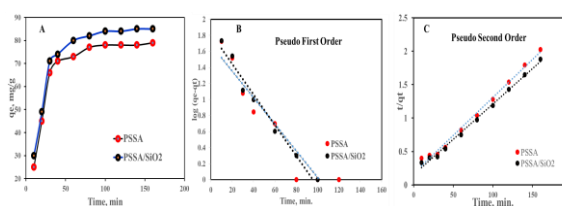


Fig. 6. Curves of adsorption kinetic of MB dye; effect of time on adsorption capacity of MB (non-linear fitting), the pseudo first order kinetic model for MB adsorption (linear fitting), and the pseudo second order kinetic model for MB adsorption ((linear fitting).

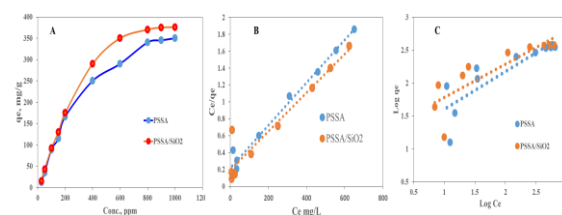


Fig. 7. Curves of isothermal MB dye adsorption; effect of concentration of MB on the adsorption (non-linear fitting), Langmuir model for MB adsorption (linear fitting), and Freundlich model for MB adsorption (linear fitting).

According to our results, a pseudo second-order kinetic model gives the most accurate reflection of the adsorption mechanism. (Fig. 6B) The first order kinetic fitting (Eq. 3) was generally not satisfactory across the full range of contact time. PSSA and PSSA/SiO<sub>2</sub> had pseudo first-order model correlation coefficients of 0.90 and 0.97, respectively. Moreover, the calculated equilibrium adsorption amounts ( $q_{e,cal}$ ) differed greatly from the experimental results ( $q_{e,exp}$ ). This suggests that the adsorption system has not followed the pseudo first-order equation [31,32]. Based on adsorption kinetics data described with pseudo-second-order model, bi-atomic adsorption mechanism seems to occur during adsorption process, which involves both adsorbent and adsorbate

functional groups [34]. As a result of fitting of a pseudo second-order model (eq. 4) to both PSSA and PSSA/SiO<sub>2</sub> adsorption kinetic data was obtained with correlation coefficients ( $R^2$  0.991 and 0.996, respectively). Also, the experimental ( $q_{e,exp}$ ) and calculated ( $q_{e,calc}$ ) adsorption capacities were very similar.

### 3.6. Adsorption isotherms

Adsorption isotherms are used to analyze adsorption processes, such as the amount of material adsorbed on the surface of the nanocomposites. Two types of isotherm models have been used to determine PSSA and PSSA/SiO<sub>2</sub> isotherms, Langmuir equation 5 and Freundlich equation 6.

$$\frac{C_e}{q_e} = \frac{K_s}{q_{max}} + \frac{C_e}{q_{max}} \quad \text{Eq. (5)}$$

where  $q_e$  is the MB adsorbed by the composite (mg/g),  $C_e$  is the equilibrium concentration of the dye (mg/l),  $q_{max}$  represents the maximum MB adsorbed on the hydrogel (mg/g), and  $K_s$  represents Langmuir constant (mg/l).

$$\log q_e = \frac{1}{n} \log C_e + \log P \quad \text{Eq. (6)}$$

where  $P$  describes the adsorption capacity (mg/g), and  $n$  is a constant depicting the adsorption intensity (dimensionless).

Figure 7 illustrates the results of isotherm studies of the adsorption process at different initial MB concentrations (ranging from 25 mg/L to 1000 mg/L). According to Langmuir, the adsorption takes place on a monolayer, with homogeneous adsorption sites. A Freundlich model suggests that adsorbents have multilayer sites on heterogeneous surfaces. In order to achieve adsorption equilibrium, the adsorption rate must be equal to the desorption rate. Figure 7 (B, C) illustrates Langmuir and Freundlich's adsorption isotherms. In table 2, the fitting parameters for both isotherm models were achieved. As a result, Langmuir maximum adsorption capacities for the PSSA and PSSA/SiO<sub>2</sub> were found to be 400 mg/g and 434 mg/g respectively. Further, the Langmuir model shows better fitting coefficients of correlation ( $R^2 > 0.98$  and 0.91), indicating that the adsorbed MB formed monolayers by direct interaction with energetically equivalent adsorption sites on PSSA and PSSA/SiO<sub>2</sub>.

### 3.7. Desorption study

It is very important to reuse adsorbent materials in industrial fields. We tested the properties of the PSSA and PSSA/SiO<sub>2</sub> by repeating the adsorption and desorption cycles four times. The results are displayed in Figure (8). As a result of the fourth cycle, the adsorption capacity of PSSA and PSSA/SiO<sub>2</sub> was reduced slightly from 98 to 93. The conclusion is that cationic dyes can be effectively removed via regeneration of PSSA and PSSA/SiO<sub>2</sub>.

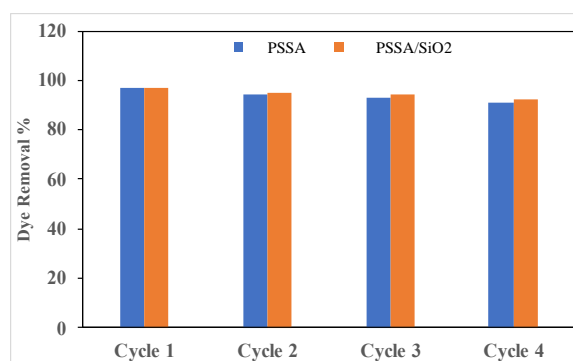


Fig. 8. Reusability of PSSA and PSSA/SiO<sub>2</sub> composites for MB adsorption.

## 4. Conclusion

In this study, a simple, effective, and inexpensive method is developed for recycling waste expanded polystyrene by synthesizing polystyrene sulphonic acid (PSSA). Polystyrene sulfonic acid has been used for the preparation of polystyrene composites with silicon dioxide in three percentages 5%, 10%, and 20% respectively. The chemical composition of the prepared materials was confirmed by FT-IR, <sup>1</sup>H-NMR, and <sup>13</sup>C-NMR spectroscopic analysis. The morphology structure of the obtained polymers was investigated by scanning electron microscopy (SEM). Furthermore, the crystallinity of the PSSA and their composites was observed through XRD and its thermal stability was examined by using thermogravimetry (TG) processes. The result indicates the formation of PSSA composites improved the surface morphology, crystallinity and thermal stability of PSSA. In order to remove methylene blue dye from water, PSSA and PSSA/10% SiO<sub>2</sub> were tested. PSSA/10% SiO<sub>2</sub> performed better in terms of

absorption than PSSA. A pseudo-second-order kinetic equation fits well the adsorption properties of the composite. Adsorption is better described by the Langmuir isotherm than by the Freundlich isotherm according to the isotherm studies. As a result of

PSSA/10% SiO<sub>2</sub>, the maximum adsorption was 434 mg/g. In conclusion, the PSSA/10% SiO<sub>2</sub> adsorbent can be used as an alternative to remove organic pollutants from an aqueous environment in an economical and efficient manner.

### Declarations

Conflict of interest The authors declare that they have no known competing financial interests or personal relationships that could have appeared to influence the work reported in this paper.

### Authors Contributions

All authors contributed equally to this work.

### Competing Interests

The authors declare no conflict of interest.

### Acknowledgement

The authors wish to thank National Research Center, Giza, Egypt and South Valley University, Qena, Egypt for their financial support

### References

- [1] He X, Male KB, Nesterenko PN, Brabazon D, Paull B, Luong JHT. Adsorption and desorption of methylene blue on porous carbon monoliths and nanocrystalline cellulose. *ACS Appl Mater Interfaces* 2013;5:8796–804. <https://doi.org/10.1021/am403222u>.
- [2] Salama A, Abouzeid R, Leong WS, Jeevanandam J, Samyn P, Dufresne A, et al. Nanocellulose-based materials for water treatment: Adsorption, photocatalytic degradation, disinfection, antifouling, and nanofiltration. *Nanomaterials* 2021;11:3008. <https://doi.org/10.3390/nano11113008>.
- [3] Abouzeid RE, Khiari R, El-Wakil N, Dufresne A. Current State and New Trends in the Use of Cellulose Nanomaterials for Wastewater Treatment. *Biomacromolecules* 2019;20:573–97. <https://doi.org/10.1021/acs.biomac.8b00839>.
- [4] Salama A, Hesemann P. Synthesis of N-Guanidinium-Chitosan/Silica Hybrid Composites: Efficient Adsorbents for Anionic Pollutants. *J Polym Environ* 2018;26:1986–97. <https://doi.org/10.1007/s10924-017-1093-3>.
- [5] Hao Y, Cui Y, Peng J, Zhao N, Li S, Zhai M. Preparation of graphene oxide/cellulose composites in ionic liquid for Ce (III) removal. *Carbohydr Polym* 2019;208:269–75. <https://doi.org/10.1016/j.carbpol.2018.12.068>.
- [6] Dong YD, Zhang H, Zhong GJ, Yao G, Lai B. Cellulose/carbon Composites and their Applications in Water Treatment – a Review. *Chem Eng J* 2021;405. <https://doi.org/10.1016/j.cej.2020.126980>.
- [7] Yu J, Wang AC, Zhang M, Lin Z. Water treatment via non-membrane inorganic nanoparticles/cellulose composites. *Mater Today* 2021. <https://doi.org/10.1016/j.mattod.2021.03.024>.
- [8] Owda ME, Elfeky AS, Abouzeid RE, Saleh AK, Awad MA, Abdellatif HA, et al. Enhancement of photocatalytic and biological activities of chitosan/activated carbon incorporated with TiO<sub>2</sub> nanoparticles. *Environ Sci Pollut Res* 2021. <https://doi.org/10.1007/s11356-021-17019-y>.
- [9] Hassan ML, Fadel SM, Abouzeid RE, Abou Elseoud WS, Hassan EA, Berglund L, et al. Water purification ultrafiltration membranes using nanofibers from unbleached and bleached rice straw. *Sci Rep* 2020;10. <https://doi.org/10.1038/s41598-020-67909-3>.
- [10] Ali KA, Wahba MI, Abou-Zeid RE, Kamel S. Development of carrageenan modified with nanocellulose-based materials in removing of Cu<sup>2+</sup>, Pb<sup>2+</sup>, Ca<sup>2+</sup>, Mg<sup>2+</sup>, and Fe<sup>2+</sup>. *Int J Environ Sci Technol* 2019;16:5569–76. <https://doi.org/10.1007/s13762-018-1936-z>.
- [11] Sinha V, Patel MR, Patel J V. Pet waste management by chemical recycling: A review. *J Polym Environ* 2010;18:8–25. <https://doi.org/10.1007/s10924-008-0106-7>.
- [12] Dacrory S, Abou-Yousef H, Abouzeid RE, Kamel S, Abdel-aziz MS, El-badry M. Antimicrobial cellulosic hydrogel from olive oil industrial residue. *Int J Biol Macromol* 2018;117:179–88. <https://doi.org/10.1016/j.ijbiomac.2018.05.179>.
- [13] Salama A. New sustainable hybrid material as adsorbent for dye removal from aqueous solutions. *J Colloid Interface Sci* 2017;487:348–53. <https://doi.org/10.1016/j.jcis.2016.10.034>.
- [14] Salama A. Cellulose/calcium phosphate hybrids: New materials for biomedical and environmental applications. *Int J Biol Macromol* 2019;127:606–17. <https://doi.org/10.1016/j.ijbiomac.2019.01.130>.
- [15] Abou-Zeid RE, Salama A, Al-Ahmed ZA, Awwad NS, Youssef MA. Carboxylated cellulose nanofibers as a novel efficient adsorbent for water purification. *Cellul Chem Technol* 2020;54:237–45. <https://doi.org/10.35812/CELLULOSECHEMTECHNOL.2020.54.25>.
- [16] Abou-Zeid RE, Dacrory S, Ali KA, Kamel S. Novel method of preparation of tricarboxylic cellulose nanofiber for efficient removal of heavy metal ions from aqueous solution. *Int J Biol Macromol* 2018;119:207–14.

- <https://doi.org/10.1016/j.ijbiomac.2018.07.127>.
- [17] Bhatti HN, Safa Y, Yakout SM, Shair OH, Iqbal M, Nazir A. Efficient removal of dyes using carboxymethyl cellulose/alginate/polyvinyl alcohol/rice husk composite: Adsorption/desorption, kinetics and recycling studies. *Int J Biol Macromol* 2020;150:861–70. <https://doi.org/10.1016/j.ijbiomac.2020.02.093>.
- [18] Hassan M, Hassan E, Fadel SM, Abou-Zeid RE, Berglund L, Oksman K. Metallo-Terpyridine-Modified Cellulose Nanofiber Membranes for Papermaking Wastewater Purification. *J Inorg Organomet Polym Mater* 2018;28:439–47. <https://doi.org/10.1007/s10904-017-0685-7>.
- [19] Hassan H, Salama A, El-ziaty AK, El-Sakhawy M. New chitosan/silica/zinc oxide nanocomposite as adsorbent for dye removal. *Int J Biol Macromol* 2019;131:520–6. <https://doi.org/10.1016/j.ijbiomac.2019.03.087>.
- [20] Salama A, Hesemann P. New N-guanidinium chitosan/silica ionic microhybrids as efficient adsorbent for dye removal from waste water. *Int J Biol Macromol* 2018;111:762–8. <https://doi.org/10.1016/j.ijbiomac.2018.01.049>.
- [21] Jawad AH, Abdulhameed AS, Malek NNA, ALOthman ZA. Statistical optimization and modeling for color removal and COD reduction of reactive blue 19 dye by mesoporous chitosan-epichlorohydrin/kaolin clay composite. *Int J Biol Macromol* 2020;164:4218–30. <https://doi.org/10.1016/j.ijbiomac.2020.08.201>.
- [22] Jawad AH, Mubarak NSA, Abdulhameed AS. Tunable Schiff's base-cross-linked chitosan composite for the removal of reactive red 120 dye: Adsorption and mechanism study. *Int J Biol Macromol* 2020;142:732–41. <https://doi.org/10.1016/j.ijbiomac.2019.10.014>.
- [23] Salama A, Abou-Zeid RE. Ionic chitosan/silica nanocomposite as efficient adsorbent for organic dyes. *Int J Biol Macromol* 2021;188:404–10. <https://doi.org/10.1016/j.ijbiomac.2021.08.021>.
- [24] Fabryanty R, Valencia C, Soetaredjo FE, Putro JN, Santoso SP, Kurniawan A, et al. Removal of crystal violet dye by adsorption using bentonite – alginate composite. *J Environ Chem Eng* 2017;5:5677–87. <https://doi.org/10.1016/j.jece.2017.10.057>.
- [25] Abou-Zeid RE, Awwad NS, Nabil S, Salama A, Youssef MA. Oxidized alginate/gelatin decorated silver nanoparticles as new nanocomposite for dye adsorption. *Int J Biol Macromol* 2019;141:1280–6. <https://doi.org/10.1016/j.ijbiomac.2019.09.076>.
- [26] Abou-Zeid RE, Ali KA, Gawad RMA, Kamal KH, Kamel S, Khiari R. Removal of cu(Ii), pb(ii), mg(ii), and fe(ii) by adsorption onto alginate/nanocellulose beads as bio-sorbent. *J Renew Mater* 2021;9:601–13. <https://doi.org/10.32604/jrm.2021.014005>.
- [27] Dong A, Xie J, Wang W, Yu L, Liu Q, Yin Y. A novel method for amino starch preparation and its adsorption for Cu(II) and Cr(VI). *J Hazard Mater* 2010;181:448–54. <https://doi.org/10.1016/j.jhazmat.2010.05.031>.
- [28] Mousa HM, Fahmy HS, Abouzeid R, Abdel-Jaber GT, Ali WY. Polyvinylidene fluoride-cellulose nanocrystals hybrid nanofiber membrane for energy harvesting and oil-water separation applications. *Mater Lett* 2022;306. <https://doi.org/10.1016/j.matlet.2021.130965>.
- [29] Liu D, Cabrera J, Zhong L, Wang W, Duan D, Wang X, et al. Using loose nanofiltration membrane for lake water treatment: A pilot study. *Front Environ Sci Eng* 2021. <https://doi.org/10.1007/s11783-020-1362-6>.
- [30] Hassan E, Hassan M, Abou-zeid R, Berglund L, Oksman K. Use of bacterial cellulose and crosslinked cellulose nanofibers membranes for removal of oil from oil-in-water emulsions. *Polymers (Basel)* 2017;9. <https://doi.org/10.3390/polym9090388>.
- [31] Park CH, Jeon HS, Yu HS, Han OH, Park JK. Application of electrostatic separation to the recycling of plastic wastes: Separation of PVC, PEL and ABS. *Environ Sci Technol* 2008;42:249–55. <https://doi.org/10.1021/es070698h>.
- [32] Howell SG. A ten year review of plastics recycling. *J Hazard Mater* 1992;29:143–64. [https://doi.org/10.1016/0304-3894\(92\)85066-A](https://doi.org/10.1016/0304-3894(92)85066-A).
- [33] Sastri VR. Chapter 6 - Commodity Thermoplastics: Polyvinyl Chloride, Polyolefins, and Polystyrene. *Plast. Med. devices Prop. requirements Appl.*, 2014, p. 73–119.
- [34] Adnan, Shah J, Jan MR. Recovery of Valuable Hydrocarbons from Waste Polystyrene Using Zinc Supported Catalysts. *J Polym Environ* 2017;25:759–69. <https://doi.org/10.1007/s10924-016-0858-4>.
- [35] Mo Y, Zhao L, Chen CL, Tan GYA, Wang JY. Comparative pyrolysis upcycling of polystyrene waste: Thermodynamics, kinetics, and product evolution profile. *J Therm Anal Calorim* 2013;111:781–8. <https://doi.org/10.1007/s10973-012-2464-6>.
- [36] Salhofer S, Schneider F, Obersteiner G. The ecological relevance of transport in waste disposal systems in Western Europe. *Waste Manag* 2007;27. <https://doi.org/10.1016/j.wasman.2007.02.025>.